*Int. J. Electrochem. Sci.*, 8 **(2013)** 9723 - 9733

International Journal of
ELECTROCHEMICAL
SCIENCE
www.electrochemsci.org

# Comparative Study of Carbon Black and Multi-walled Carbon Nanotubes as Conductive Additives on Electrochemical Performance of Branched CuO Nanostructures

*Yu Xin Zhang*[1,2,*], *Min Kuang*[1], *Ming Huang*[1], *Zhong Quan Wen*[2]

[1] College of Materials Science and Engineering, Chongqing University, Chongqing, 400044, P.R. China
[2] Key Laboratory of Fundamental Science of Micro/Nano-Devices and System Technology, Chongqing University, Chongqing, 400044, P.R. China
[*]E-mail: zhangyuxin@cqu.edu.cn

*Received:* 17 May 2013 / *Accepted:* 19 June 2013 / *Published:* 1 July 2013

In this work, comparative study of carbon blacks (CB) and multi-walled carbon nanotubes (MWNTs) as conductive additives, were examined to enhance electrochemical performance of dandelion-like hollow CuO (H-CuO) and flower-like CuO (F-CuO) as nanostructured electrode materials for supercapacitors. The structure and morphology of as-synthesized CuO were characterized by nitrogen adsorption, X-ray diffraction (XRD) and focus ion beam scanning electron microscopy (FIB/SEM). Furthermore, the electrochemical properties of CuO mixed with CB and MWNTs were elucidated by galvanostatic charge/discharge and cyclic voltammetric measurements. The electrochemical results demonstrated that both of branched CuO nanostructures mixed with MWNTs exhibited higher specific capacitance and stable cycling performance. Interestingly, MWNTs kept CuO from peeling during the charge/discharge process, while branched CuO nanostructures prevented MWNTs from agglomeration, thus facilitating ion transport in the electrode material. In principles, our findings could be effective for the choice of conductive additives depending on CuO morphologies (e.g., branched structures) to improve the electrochemical performance.

**Keywords:** Copper oxides; carbon conductive additives; supercapacitors; branched structure

## 1. INTRODUCTION

Supercapacitors are important electrical energy storage devices due to their high specific power density, fast recharge capabilities and long cycle life compared with batteries[1]. The development of high-performance and low-cost electrode materials for supercapacitors has attracted increased interest

in recent years. Transition metal oxides (NiO, $Co_3O_4$, CuO, $FeO_x$, $MnO_2$ and $V_2O_5$)[2-6], because of their favorable capacitive characteristics and environmental friendliness, are generally considered as promising electrode materials for supercapacitors. Among the transition metal oxides, CuO has attractive features like low cost, abundant resources, non-toxicity, and easy preparation in diverse shapes with nanosized dimension [7, 8]. It has been widely investigated as electrode material for rechargeable Li-ion batteries[9]. Recently, the supercapacitance behavior of CuO has attracted research interest. For instance, Dubal et al. [10] reported that copper oxide multilayer nanosheets thin films with a specific capacitance of 43 F $g^{-1}$ in 1 M $Na_2SO_4$ electrolyte. Zhang et al. [11] prepared CuO nanobelts with high surface area, and small crystal grains displayed a specific capacitance of 62 F $g^{-1}$ in 1 M $LiPF_6$/EC:DEC electrolyte. Patake et al. [12] synthesized the porous amorphous copper oxide thin films which exhibited a specific capacitance of 36 F $g^{-1}$ in 1 M $Na_2SO_4$ electrolyte. Zhang et al. [13] reported that CuO with flower-like nanostructures showed a specific capacitance of 133.6 F $g^{-1}$ in 1 M KOH electrolyte, however, the specific capacitance of CuO was still low and exhibited unstable cycling performances.

On the other hand, the conductivity of electrodes has a great influence on the pseudocapacitance[14-16]. Pseudocapacitive material with good conductivity would show low polarization resulting in high utilization of materials and high pseudocapacitance. To increase the conductivity of electrodes, two strategies have been widely adopted: namely, (i) doping and coating of conductive phases to improve the intrinsic conductivity of active materials; and (ii) incorporation of conductive additives into the electrodes to form conductive networks around the active materials[17-20]. Among a variety of carbon materials, CB was the most popular conductive additive because of its low cost, reasonably high electrical conductivity and high durability after long cyclic loading. Having a spherical shape with a typical diameter of tens of nanometers, however, made it difficult for CB particles to form an extensive 'point to point' conductive network. Taking advantages of their extremely high aspect ratios and electrical conductivities, nanocarbon materials, such as carbon nanotubes and graphene nanosheets, have been extensively studied as conductive additives, aiming at constructing conductive networks at a lower percolation threshold[21]. However, graphene remained a relatively new topic that was mainly limited to academic research[22]. On the contrary, active materials employing MWNTs were much closer to commercialization.

In this work, the effects of carbon blacks (CB) and multi-walled carbon nanotubes (MWNTs) on the performance of branched CuO-based electrodes were comparatively investigated. The influence of carbonaceous conductive additives in different dimensions on the branch-structure CuO was studied. Meanwhile, the mechanism of enhancement in conductivity was further discussed.

## 2. EXPERIMENTAL SECTION

### *2.1 Materials*

Copper nitrate ($Cu(NO_3)_2 \cdot 3H_2O$), sodium hydrate (NaOH), ammonia ($NH_3 \cdot H_2O$), ethanol ($C_2H_5OH$), polyvinylidene fluoride (PVDF) and solvents used in this work were purchased fromAlfa

Aesar. The MWNTs and CB particles were provided by Jiangxi Battery Co. Ltd. (Jiangxi, China). The entire chemicals were of analytical purity and used without any further purification.

### *2.2 Synthesis of CuO products*

The H-CuO microspheres were obtained by a hydrothermal method [23]. A starting solution of copper (0.1 M) was prepared by mixing $Cu(NO_3)_2 \cdot 3H_2O$ in pure ethanol solvent. A portion of above solution (15 ml) was added to ammonia solution (15 ml, 25-28%), followed by addition of 5 ml NaOH (1.0 M). After stirring for 10 min to form a clear solution, the resulting solution was transferred into a 50 mL stainless-steel autoclaves lined with poly(tetrafluoroethylene) (PTFE, Telfon). The autoclave was sealed and maintained at 453 K for 5 h and then cooled down to room temperature. The resulting precipitate solid were collected by centrifugation, washed with distilled water and absolute ethanol, and finally dried at 333 K. Meanwhile, the flower-like CuO (F-CuO) prepared by our recent work[24] was also used as electrode materials to systematically investigated the influence of CB and MWNTs.

### *2.3 Materials Characterization*

The crystallographic information of as-prepared products was established by powder X-ray diffraction (XRD, D/max 1200, Cu Kα). The structure and morphology of the products were carried out with focused ion beam scanning electron microscopy (Zeiss Auriga FIB/SEM). Nitrogen adsorption-desorption isotherms were measured at 77 K with micrometritics ASAP 2020 sorptometer. Before test, the samples were oven-dried at 333 K for 8 h under vacuum condition. The specific surface area was calculated using the Brunauer-Emmett-Teller (BET) method based on adsorption data in the partial pressure ($P/P_0$) range of 0.05 to 0.30.

### *2.4 Electrochemical measurements*

To investigate the impacts of different conductive additives on H-CuO and F-CuO capacitance performance, cyclic voltammetry (CV) and galvanostatic charge-discharge (GC) tests were performed by using a CHI 660E electrochemical workstation at room temperature. All electrochemical measurements were conducted in 6.0 M KOH aqueous solution. In a typical electrochemical measurement, a three-electrode cell system was composed of CuO powders electrode as the working electrode, a platinum plate as the counter electrode, and a saturated calomel electrode as the reference electrode. The working electrode was fabricated by mixing the 70 wt% as-prepared CuO with 20 wt% CB or MWNTs and 10 wt% polyvinylidene fluoride (PVDF), and then a slurry of above mixture was painted onto the foamed nickel as a current collector. The coated mesh was dried at 393 K in vacuum cabinet overnight to remove the solvent and water.

The composite positive electrodes were investigated by cyclic voltammetry technique with varying the potential between 0 and 0.4 V at a rate of 5-50 mV $s^{-1}$. The charge-discharge current densities ranged from 2 to 10 mA $cm^{-2}$ at a potential of 0 to 0.4 V.

## 3. RESULTS AND DISCUSSION

### *3.1 Structure and morphology of branched CuO nanostructures*

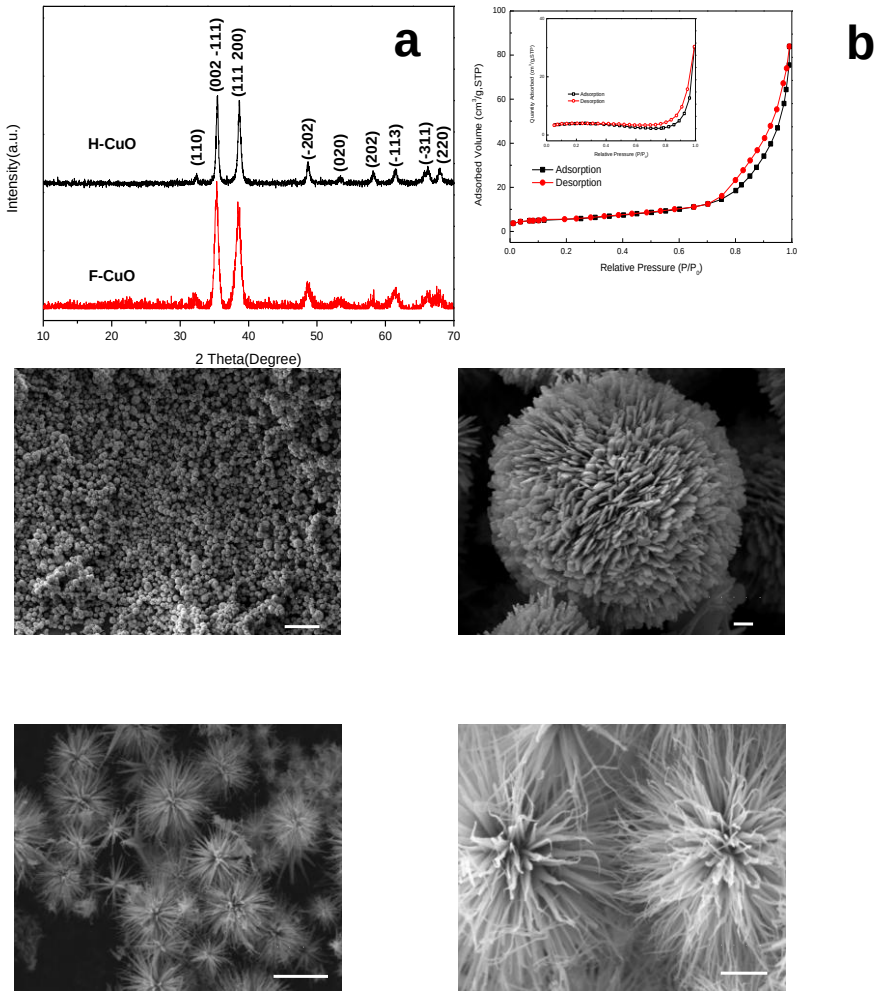


**Figure 1.** XRD pattern of the H-CuO and F-CuO (a). (b) $N_2$ adsorption desorption isotherms of H-CuO (Inset is the isotherms of F-CuO). SEM images of H-CuO (c, d); F-CuO (e, f).

**Table 1.** BET surface area ( $S_{BET}$) and pore volume ( V ) for H-CuO and F-CuO in this work.

| | | V ($cm^3$/g) | | | |
|---|---|---|---|---|---|
| Sample | $S_{BET}$ ($m^2$/g) | Total | Micro- (< 2 nm) | Meso- (2-50 nm) | Macro- ( > 50 nm) |
| H-CuO | 22.7 | 0.0017 | 3.1% | 60.6% | 36.3% |
| F-CuO | 12.2 | 0.0061 | 34.3% | 63.8% | 1.9% |

Fig. 1a shows the XRD patterns of the products H-CuO and F-CuO, indicating a high degree of crystallinity with all reflections indexed to the monoclinic CuO (JCPDS card no. 48-1548). Fig. 1b

presents their surface area and porosity properties, and the analytical results are listed in Table 1 for reference.

The $N_2$ adsorption/desorption isotherms exhibited hysteresis loops in the relative pressure range of 0.7-1.0, which belonged to the type-IV[25, 26]. The BET surface areas were 19.2 $m^2$ $g^{-1}$ for H-CuO and 12.1 $m^2$ $g^{-1}$ for F-CuO. The morphology of H-CuO microspheres was characterized by SEM (Fig. 1c-1d), the diameters of which mainly ranged from 3 to 5 μm. Clearly, all of these H-CuO spheres had a highly porous, flocky appearance and resulted from self-assembly of nanoplates with an average thickness of about 10-20 nm (Fig. 1d); these nanoplates interweaved together forming an open porous structure and were expected to facilitate electrolyte penetration into the electrode particles, thus providing more interface area between the electrode materials and the electrolyte. The low magnified image (Fig. 1e) indicates that the panoramic morphology of the F-CuO is hierarchically flower-like, with a diameter ranging from 1 to 2 μm. The clear view (Fig. 1f) shows that the surface of the F-CuO is not smooth and consists of nanobranches with average widths of 5 to 10 nm. Thus, the product was considered to be a 3D hierarchical micro/nanostructure.

*3.2 Electrochemical properties of H-CuO-CB and H-CuO-MWNTs*

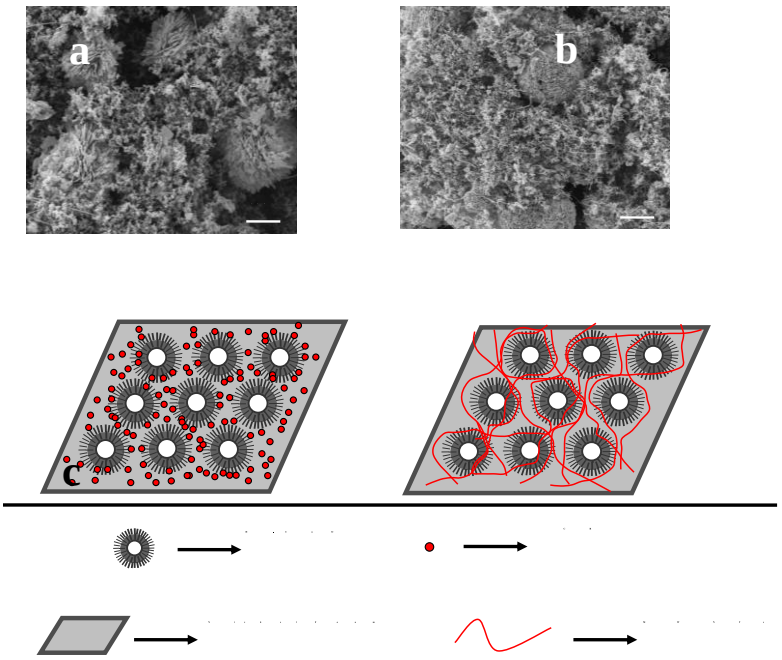


**Figure 2.** The morphology of the H-CuO-based electrode materials: (a) H-CuO-CB; (b) H-CuO-MWNTs. (c) The diagram of conductive network simulation.

Fig. 2a and 2b show the morphology of H-CuO-CB and H-CuO-MWNTs, respectively. As known, conductive additives provided conductive path from the current collector to the active material through the electrodes. It was noticed that CB were gathered into the spaces between the H-CuO microspheres (Fig. 2a), and could not formAn effective conductive network when they were mixed. However, MWNTs had vimineous fibre shape and winded with CuO microspheres. Based on the morphologies of various carbons and composites, a possible conductive mechanism of different conductive additives for H-CuO was developed as shown in Fig. 2c. Obviously, fibrous additives of MWNTs cannot only form a good conductive network, but also keep CuO microspheres from peeling during the charge/discharge process, similar to the function of fibre reinforced concrete.

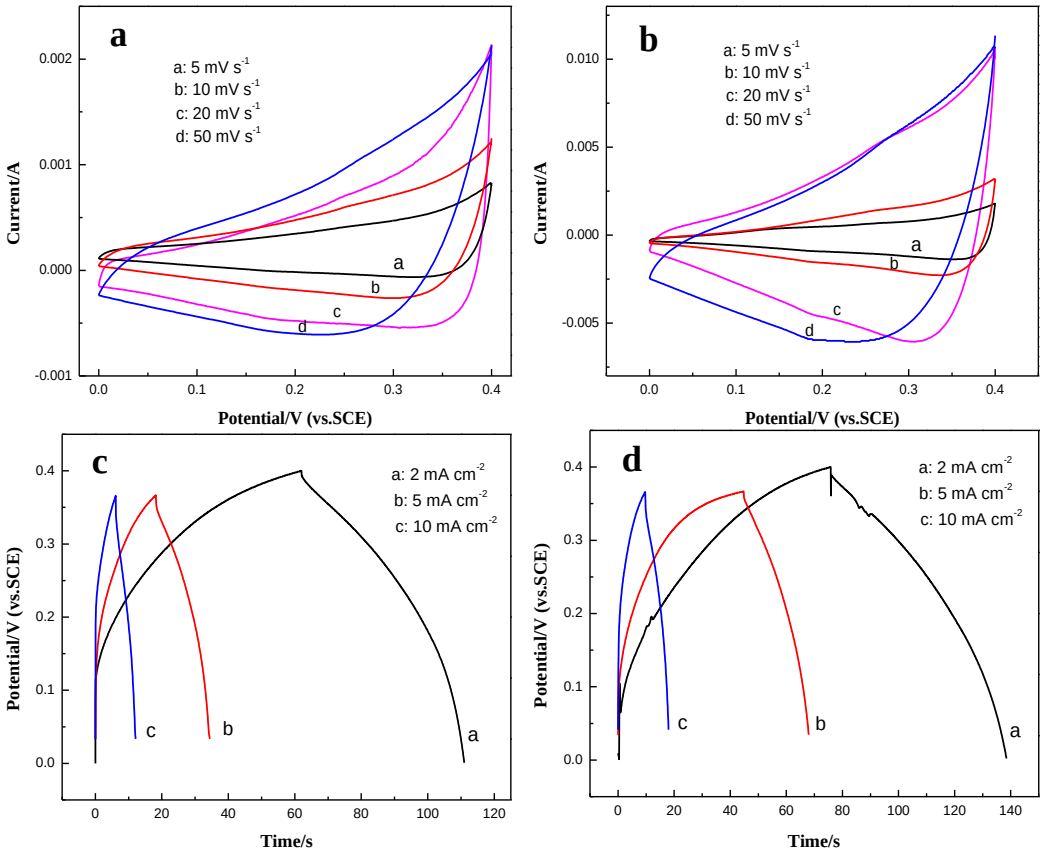


**Figure 3.** Cyclic voltammetry experiments within 0.0-0.4 V at a scan rate from 5.0 to 50 mV $s^{-1}$ for H-CuO-CB (a) and H-CuO-MWNTs (b) electrodes in 6 mol $L^{-1}$ KOH electrolytes at room temperature. The galvanostatic charge-discharge curves of H-CuO-CB (c) and H-CuO-MWNTs (d) for current densities of 2, 5 and 10 mA $cm^{-2}$ in 6 mol $L^{-1}$ KOH electrolytes at room temperature.

As shown in Fig. 3a and 3b, the CV curves of H-CuO-CB and H-CuO-MWNTs exhibit difference shapes from that of electric double layer capacitance, suggesting that the capacity mainly resulted from pseudocapacitive capacitance [27, 28]. However, the unobvious redox peaks may result from the high resistivity of H-CuO powders. According to the data in Fig. 3a and b, the specific capacitance of H-CuO-MWNTs was the largest one among the samples. Fig. 3c and d show

charge/discharge curves of H-CuO-CB and H-CuO-MWNTs, respectively. The nearly linear charge/discharge curves indicate a good reversibility during the charge/discharge processes. Moreover, the charge/discharge times varied at a constant current density for H-CuO-CB and H-CuO-MWNTs, suggesting different specific capacitances. According to the charge/discharge curves, the specific capacitance ($C_m$) of electrodes can be calculated according to the following equation:

$$C_m = \frac{I\Delta t}{m\Delta V}$$

where I (mA) is the discharge current for the applied time duration Δt (s), ΔV (V) is the potential window, and m is the weight of H-CuO. The specific capacitances for H-CuO-CB and H-CuO-MWNTs are summarized in Fig. 4a. H-CuO-MWNTs yielded the high specific capacitance at a constant current density. For example, the specific capacitance of H-CuO-MWNTs was as high as 85 F $g^{-1}$ at a current density of 2 mA $cm^{-2}$, higher than 62 F $g^{-1}$ for H-CuO-CB.

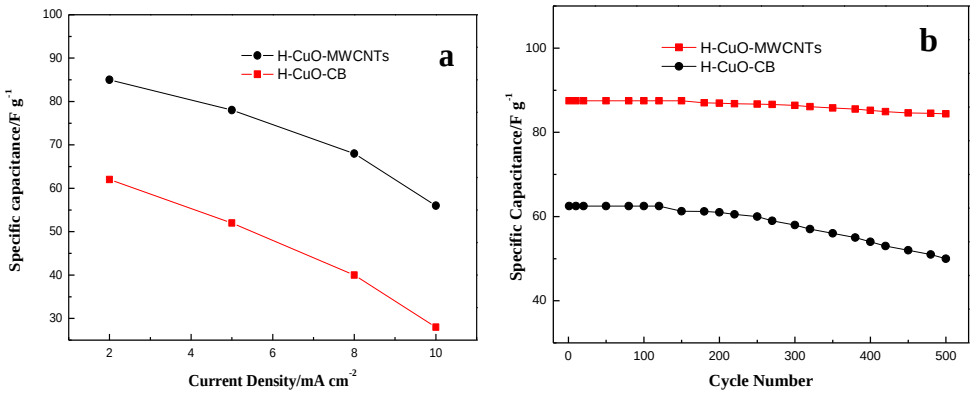


**Figure 4.** (a) Specific capacitance of H-CuO nanostructures measured under different current density; (b) Cycling performance for different H-CuO electrodes at a current density of 5 mA $cm^{-2}$ in 6 M KOH.

Although the specific capacitance of H-CuO-CB was comparable to the H-CuO-MWNTs at a low current density, the specific capacitance quickly decreased to 28 F $g^{-1}$ when the current density was increased to 10 mA $cm^{-2}$. The capacitive retention of H-CuO-CB was only about 45%, indicating a poor rate capability. For sample of H-CuO-MWNTs, the capacitive retention is about 66%, suggesting significantly improved rate capability. The drop might be explained by an ion-exchange mechanism [10]. The $OH^-$ needed enough time to transfer between the solutions into the surface of electrode materials in order to be intercalated/extracted into/out of activated materials when charging/discharging. If the scan rate was as low as 2 mA $cm^{-2}$, $OH^-$ had enough time to transfer, and much more charge transferred at a high scan rate, which meant that more charge could be stored and thus led to a higher specific capacitance.

It was also very important for electrode materials to have good specific capacitance retention. Supercapacitors should work steadily and safely, which required the specific capacitance of electrode materials to change as little as possible. Thus the cycling stability of the H-CuO-CB and H-CuO-MWNTs were investigated by continuous charge/discharge measurements over 500 cycles (Fig. 4b) at

a current density of 2 mA $cm^{-2}$ (within the potential range of 0-0.4 V). We found that the electrodes of CuO-MWNTs had good cycle life. After 200 continuous charge/discharge cycles, H-CuO-MWNTs had almost the same specific capacitance as its initial value, while the others began to decline. H-CuO-MWNTs still had more than 99% specific capacitance after 200 continuous charge/discharge cycles. Even after 500 continuous charge/discharge cycles, H-CuO-MWNTs had maintained more than 97.6% of its initial value and its specific capacitance was about 83 F $g^{-1}$, while the CuO-CB have maintained 80% of its initial value. These results indicated that the H-CuO-MWNTs were very promising candidate as electrode material than H-CuO-CB. As a consequence, the capacitance and power characteristics of CuO have been improved greatly by using MWNTs as the conductive additive. Similar phenomena were also found in batteries[29-31].

*3.3 Electrochemical properties of F-CuO-CB and F-CuO-MWNTs*

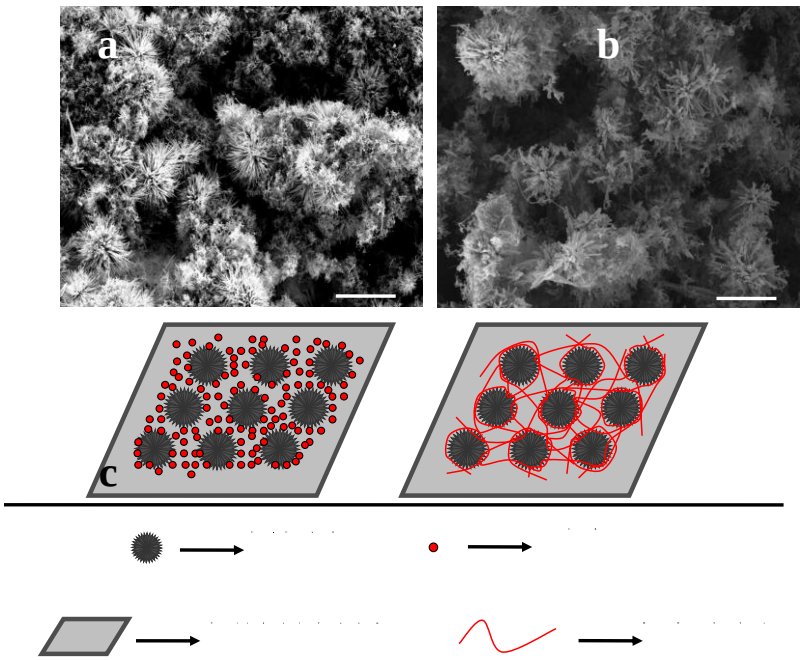


**Figure 5.** The morphology of the F-CuO-based electrode materials: (a) F-CuO-CB; (b) F-CuO-MWNTs. (c) Schemes of conductive mechanism for different conductive additives.

Fig. 5a and b presented fairly homogeneous electrodes, when MWNTs was used as conductive agents. It seemed that the MWNTs entangling among nanobranches of F-CuO (10-20 nm), and the nanobranches greatly improved the dispersibility of MWNTs. On the contrary, the special structure of

F-CuO did not make the CB homogeneously dispersed in the electrode (Fig. 5a and 5c). The presence of large localized agglomerates increased the percolation threshold [22].

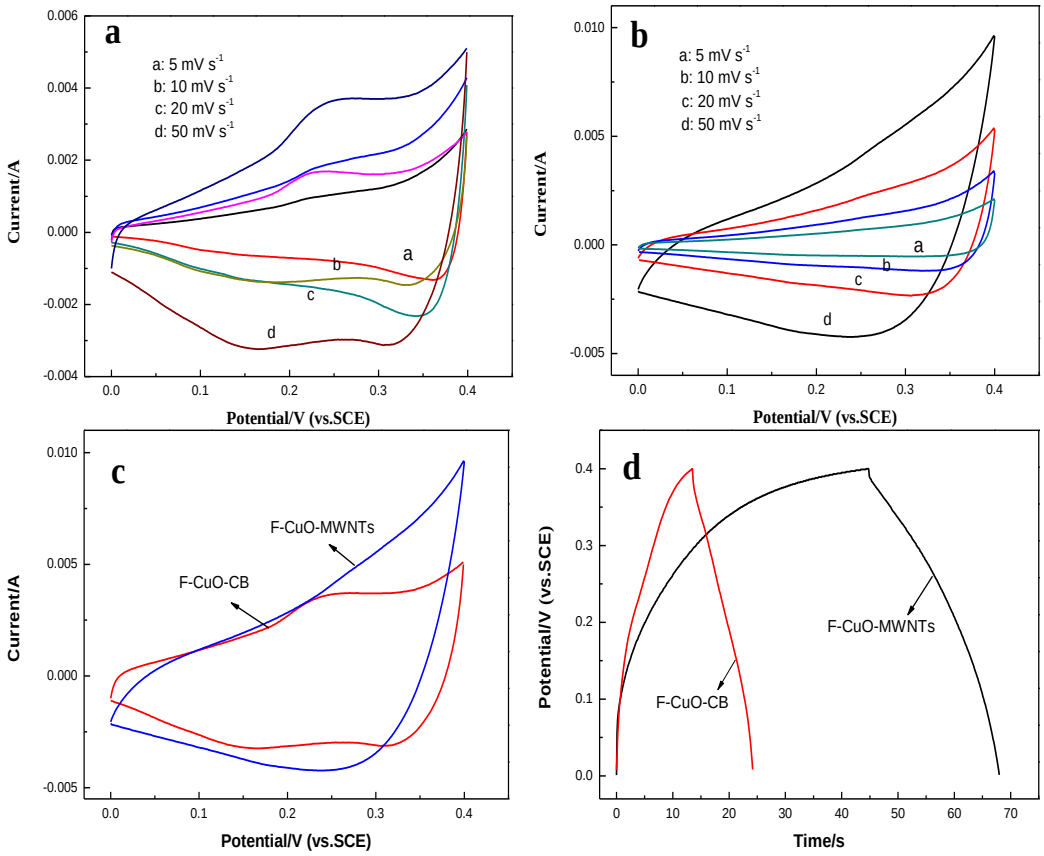


**Figure 6.** Cyclic voltammetry experiments within 0.0-0.4 V at a scan rate from 5.0 to 50 mV $s^{-1}$ for F-CuO-CB (a) and F-CuO-MWNTs (b) electrodes in 6 mol $L^{-1}$ KOH electrolytes at room temperature; (c) CV curves of F-CuO-CB and F-CuO-MWNTs at a scan rate of 50 mV $s^{-1}$; (d) The galvanostatic charge-discharge curves of F-CuO-CB and F-CuO-MWNTs at 2 mA $cm^{-2}$ in 6 mol $L^{-1}$ KOH electrolytes at room temperature.

Fig. 6 shows cyclic voltammograms and charge-discharge curves of F-CuO-CB and F-CuO-MWNTs electrode in 6 mol $L^{-1}$ KOH electrolytes with different scan rate. Clearly, it can be seen that the pseudocapacitance behavior existed in the electrodes which corresponded to the redox process between $Cu^{2+}$ and $Cu^{1+}$[12]. The CV curves on the positive scan followed the same trace completely, indicating the repeated applications of CV in the potential region of investigation and the highly reversible feature of F-CuO. Meanwhile, the cathodic currents increased slightly as the CV of positive polarization cut-off attained a further positive value of 0.4 V. The CV curves in Fig. 6a show low level current separation between anodic and cathodic currents relative to F-CuO-MWNTs, suggesting the poor electrochemical performance of F-CuO-CB. Furthermore, Fig. 6c and 6d revealed that the capacitance of F-CuO-MWNTs was also better than that of F-CuO-CB.

As mentioned above, the superiority of conductive additive to enhance the electrochemical performance of different CuO powders were in turn MWNTs > CB. This was due to the MWNTs with

the unique one-dimensional linear structure that could entangle among the H-CuO and F-CuO, so it did not only form a good conductive network, but also kept CuO from peeling during the charge/discharge process. Meanwhile, the special branch-structure of CuO prevented MWNTs from agglomeration, thus facilitating ion transport in the electrode material.

Under various current densities, MWNTs had substantially improved the capacitance and power characteristics of CuO as the conductive additives because of the combination of increased conductivity, high surface area, electrolyte accessibility and mechanical properties of the composite electrode. For specific purposes, such as high-power applications, we believed that carbon nanotubes could be a better choice. Currently, the inexpensive industrial production of MWNTs could be accomplished easily. The price per gram of material, especially for MWNTs, has become low enough to justify the replacement of carbon blacks. In addition, using MWNT-based composites as conductive additives will be another promising alternative to improve performance and reduce cost.

## 4. CONCLUSIONS

In principles, comparative study of carbon black and multi-walled carbon nanotubes as conductive additives on electrochemical performance of branched CuO nanostructures were investigated to find out that the unique characteristics of MWNTs and branched CuO nanostructure could be the main reason for a higher electrochemical performance. Although the selection of the proper conductive additive for positive electrodes involved many parameters, our findings could be effective for the choice of conductive additives depending on CuO morphologies (e.g., branched structures) to improve the electrochemical performance.

ACKNOWLEDGEMENTS

The authors gratefully acknowledge the financial supports provided by National Natural Science Foundation of China (Grant no. 51104194), Doctoral Fund of Ministry of Education of China (20110191120014), No. 43 Scientific Research Foundation for the Returned Overseas Chinese Scholars, State Education Ministry and Fundamental Research Funds for the Central Universities (Project no. CDJZR12248801 and CDJZR12135501, Chongqing University, PR China). Dr. Zhang would also like to thank Chongqing University for providing Talent of High Level Scientific Research Fund.

## References

1. H. Pang, Y. Ma, G. Li, J. Chen, J. Zhang, H. Zheng and W. Du, *Dalton Trans*., 41 (2012) 13284.
2. Y. Wang and I. Zhitomirsky, *Mater. Lett*., 65 (2011) 1759.
3. L. Yu, G. Zhang, C. Yuan and X. W. Lou, *Chem. Commun*., 49 (2013) 137.
4. D. P. Dubal, G. S. Gund, C. D. Lokhande and R. Holze, *ACS Appl. Mater. Interfaces*, 5 (2013) 2446.
5. Y. X. Zhang, S. Zhu, M. Dong, C. P. Liu and Z. Q. Wen, *J. Electrochem. Soc*., 8 (2013) 2407.
6. Y. Deng, Q. Zhang, Z. Shi, L. Han, F. Peng and G. Chen, *Electrochim. Acta*, 76 (2012) 495.

7. J. Chen, F. Zhang, J. Wang, G. Zhang, B. Miao, X. Fan, D. Yan and P. Yan, *J. Alloy. Compd*., 454 (2008) 268.
8. X. Jiang, T. Herricks and Y. Xia, *Nano Lett*., 2 (2002) 1333.
9. R. Sahay, P. Suresh Kumar, V. Aravindan, J. Sundaramurthy, W. Chui Ling, S. G. Mhaisalkar, S. Ramakrishna and S. Madhavi, *J. Phys. Chem*. C, 116 (2012) 18087.
10. J. Zhou, L. Ma, H. Song, B. Wu and X. Chen, *Electrochem. Commun*., 13 (2011) 1357.
11. J. Huang, H. Wu, D. Cao and G. Wang, *Electrochim. Acta*, 75 (2012) 208.
12. G. Wang, J. Huang, S. Chen, Y. Gao and D. Cao, *J. Power Sources*, 196 (2011) 5756.
13. Y. X. Zhang, M. Huang, M. Kuang, C. P. Liu, J. L. Tan, M. Dong, Y. Yuan, X. L. Zhao and Z. Wen, *Int. J. Electrochem. Soc*., 8 (2013) 1366.
14. H. Zhu, Ionics, 17 (2011) 641.
15. W. R. Liu, Z. Z. Guo, W. S. Young, D. T. Shieh, H. C. Wu, M. H. Yang and N. L. Wu, *J. Power Sources*, 140 (2005) 139.
16. J. G. Smith Jr, D. M. Delozier, J. W. Connell and K. A. Watson, *Polymer*, 45 (2004) 6133.
17. J. Shao, X. Li, Q. Qu and Y. Wu, *J. Power Sources*, 223 (2013) 56.
18. A. Varzi, C. Täubert and M. Wohlfahrt-Mehrens, *Electrochim. Acta*, 78 (2012) 17.
19. X. Li, Y. Zhang, H. Song, K. Du, H. Wang, H. Li and J. Huang, *Int. J. Electrochem. Soc*., 7 (2012) 7111.
20. G. Wang, Z. Shao and Z. Yu, *Nanotechnology*, 18 (2007) 205705.
21. M. Inagaki, H. Konno and O. Tanaike, *J. Power Sources*, 195 (2010) 7880.
22. B. Zhang, Y. Yu, Y. Liu, Z. D. Huang, Y. B. He and J. K. Kim, *Nanoscale*, 5 (2013) 2100.
23. B. Liu and H. C. Zeng, *J. Am. Chem. Soc*., 126 (2004) 8124.
24. Y. X. Zhang, M. Huang, F. Li and Z. Q. Wen, *Int. J. Electrochem. Soc*., 8 (2013) XX.
25. Z. Zhang, H. Che, Y. Wang, L. Song, Z. Zhong and F. Su, *Catal. Sci. T echnol.*, 2 (2012) 1953.
26. X. Li, S. Xiong, J. Li, J. Bai and Y. Qian, *Journal of Materials Chemistry*, 22 (2012) 14276.
27. X. H. Xia, J. P. Tu, Y. Q. Zhang, Y. J. Mai, X. L. Wang, C. D. Gu and X. B. Zhao, RSC Adv., 2 (2012) 1835.
28. C. Yuan, J. Li, L. Hou, L. Yang, L. Shen and X. Zhang, *Electrochim. Acta*, 78 (2012) 532.
29. J. Lv, J. P. Tu, W. K. Zhang, J. B. Wu, H. M. Wu and B. Zhang, *J. Power Sources*, 132 (2004) 282.
30. X. D. Zhu, J. Tian, S. R. Le, N. Q. Zhang and K. N. Sun, *Mater. Lett*., 97 (2013) 113.
31. K. Wang, Y. Wu, S. Luo, X. He, J. Wang, K. Jiang and S. Fan, *J. Power Sources*, 233 (2013) 209.